

Article

# Heat Capacity of Indium or Gallium Sesqui-Chalcogenides

Květoslav Růžička<sup>1</sup> , Václav Pokorný<sup>1,2</sup> , Jan Plutnar<sup>3</sup> , Iva Plutnarová<sup>3</sup> , Bing Wu<sup>3</sup>, Zdeněk Sofer<sup>3</sup> and David Sedmidubský<sup>3,\*</sup> 

<sup>1</sup> Department of Physical Chemistry, Faculty of Chemical Engineering, University of Chemistry and Technology, Prague, Technická 5, 166 28 Prague, Czech Republic; ruzickak@vscht.cz (K.R.); pokorny@imc.cas.cz (V.P.)

<sup>2</sup> Institute of Macromolecular Chemistry, Czech Academy of Sciences, Heyrovského Nám. 2, 162 06 Prague, Czech Republic

<sup>3</sup> Department of Inorganic Chemistry, Faculty of Chemical Technology, University of Chemistry and Technology, Prague, Technická 5, 166 28 Prague, Czech Republic; jan.plutnar@vscht.cz (J.P.); iva.plutnarova@vscht.cz (I.P.); bing1.wu@vscht.cz (B.W.); zdenek.sofer@vscht.cz (Z.S.)

\* Correspondence: sedmidub@vscht.cz

**Abstract:** The chalcogenides of p-block elements constitute a significant category of materials with substantial potential for advancing the field of electronic and optoelectronic devices. This is attributed to their exceptional characteristics, including elevated carrier mobility and the ability to fine-tune band gaps through solid solution formation. These compounds exhibit diverse structures, encompassing both three-dimensional and two-dimensional configurations, the latter exemplified by the compound  $\text{In}_2\text{Se}_3$ . Sesqui-chalcogenides were synthesized through the direct reaction of highly pure elements within a quartz ampoule. Their single-phase composition was confirmed using X-ray diffraction, and the morphology and chemical composition were characterized using scanning electron microscopy. The compositions of all six materials were also confirmed using X-ray photoelectron spectroscopy and Raman spectroscopy. This investigation delves into the thermodynamic properties of indium and gallium sesqui-chalcogenides. It involves low-temperature heat capacity measurements to evaluate standard entropies and Tian–Calvet calorimetry to elucidate the temperature dependence of heat capacity beyond the reference temperature of 298.15 K, as well as the enthalpy of formation assessed from DFT calculations.

**Keywords:** In; Ga; sesqui-chalcogenides; heat capacity; enthalpy; entropy; Gibbs energy



**Citation:** Růžička, K.; Pokorný, V.; Plutnar, J.; Plutnarová, I.; Wu, B.; Sofer, Z.; Sedmidubský, D. Heat Capacity of Indium or Gallium Sesqui-Chalcogenides. *Materials* **2024**, *17*, 361. <https://doi.org/10.3390/ma17020361>

Academic Editor: Vlassios Likodimos

Received: 28 November 2023

Revised: 5 January 2024

Accepted: 8 January 2024

Published: 11 January 2024



**Copyright:** © 2024 by the authors. Licensee MDPI, Basel, Switzerland. This article is an open access article distributed under the terms and conditions of the Creative Commons Attribution (CC BY) license (<https://creativecommons.org/licenses/by/4.0/>).

## 1. Introduction

In the past decade, materials for low-energy electronics have emerged as a focal point in current material research. The family of layered chalcogenides stands out as significant candidates for the advancement of innovative electronic and optoelectronic devices, owing to their exceptional properties such as high carrier mobility, a tunable band gap through solid solution formation, and their layered structure. Sesqui-chalcogenides of indium and gallium, denoted by the general formula  $\text{M}_2\text{Ch}_3$ , exhibit diverse polymorphic forms based on their composition and synthesis procedures. Gallium sulfide possesses a monoclinic structure, while gallium selenide and telluride adopt cubic structures. Indium sulfide takes on a tetragonal form, indium selenide features a hexagonal layered structure, and indium telluride has a cubic structure. The layered van der Waals structure of  $\text{In}_2\text{Se}_3$  allows for its exfoliation down to a single-layer material [1,2].

Indium and gallium chalcogenides, particularly, hold promise for the construction of photodetectors and solar cell devices [3]; their high thermal stability is a great advantage for these applications. These materials have been synthesized in various forms, including bulk crystals from elemental sources, and thin films through chemical vapor deposition (CVD) and physical vapor deposition (PVD) methods, as well as exfoliation [4–6]. Layered indium(III) selenide, known for its semiconducting properties and ferroelectric characteristics, exhibits different structural polymorphs [7]. Nanostructures of such layered

materials can be crafted using both “top-down” methods, involving the exfoliation of bulk materials, and “bottom-up” techniques, such as the formation of colloidal nanosheets and nanoparticles [8,9].

Understanding the fundamental thermophysical properties is crucial for modeling, developing, and optimizing deposition procedures for thin films, as well as for single crystal growth. Additionally, this knowledge plays a vital role in device development, as material characteristics like heat capacity and thermal conductivity are pivotal for creating high-performance devices tailored for industrial applications.

Although the *ab initio* techniques of electronic structure calculations may offer an alternative and feasible approach to assess these characteristics, as recently demonstrated on some layered structures and interfaces [10,11], as well as on Ga and In monochalcogenides [12], the experimental data obtained on real materials are indeed highly valuable, in particular for defected and disordered structures that must be theoretically modeled by ordered superstructures. This is also the case of Ga<sub>2</sub>Se<sub>3</sub>, Ga<sub>2</sub>Te<sub>3</sub>, and In<sub>2</sub>Te<sub>3</sub>, which crystallize in a disordered zinc blende structure with 1/3 of vacancies on a cation sublattice. This approach was thus applied in this study to calculate the enthalpy of formation of Ga<sub>2</sub>Te<sub>3</sub>, while the ordered counterparts were considered for Ga<sub>2</sub>Se<sub>3</sub> and In<sub>2</sub>Te<sub>3</sub>.

## 2. Materials and Methods

### 2.1. Synthesis

Gallium, indium, sulfur, selenium, and tellurium were used in a form of granules (1–6 mm, 99.9999% purity, Wuhan XinRong New Materials Co., Wuhan, China). Gallium and indium chalcogenides of general formula M<sub>2</sub>Ch<sub>3</sub> were produced through a direct reaction from elements in a quartz ampoule under a high vacuum. Quartz ampoules with dimensions of 25 × 120 mm and a wall thickness of 3 mm were used for the synthesis of gallium selenide, gallium telluride, and all indium chalcogenides. For the synthesis of Ga<sub>2</sub>S<sub>3</sub>, an ampoule of dimensions 30 × 280 mm with a 3 mm wall thickness was used. For the synthesis, elements corresponding to 15 g of M<sub>2</sub>Ch<sub>3</sub> with a precision better than ±1 mg were placed in the ampoule, which was further evacuated to the pressure of 1 × 10<sup>−3</sup> Pa using a diffusion pump and sealed with an oxygen–hydrogen torch. The ampoules were heated at a heating rate of 5 °C/min to a temperature of about 50 °C above the melting point of the respective chalcogenide and kept at this temperature for 6 h. Subsequent cooling to room temperature was carried out at a rate of 0.2 °C/min. The maximum synthesis temperatures were 1050 °C for Ga<sub>2</sub>S<sub>3</sub> and Ga<sub>2</sub>Se<sub>3</sub>, 850 °C for Ga<sub>2</sub>Te<sub>3</sub>, 950 °C for In<sub>2</sub>Se<sub>3</sub>, 1100 °C for In<sub>2</sub>S<sub>3</sub>, and 720 °C for In<sub>2</sub>Te<sub>3</sub>. A longer ampoule was used for the synthesis of Ga<sub>2</sub>S<sub>3</sub> and the cold part of the ampoule was kept at 500 °C to avoid a high pressure of gaseous sulfur, since the reaction of elemental gallium and sulfur only occurs at temperatures exceeding 800 °C. The ampoules were opened in an argon atmosphere (glovebox) and the products were ground inside the glovebox using an agate mortar and pestle and sieved to a particle size of −100 mesh. In<sub>2</sub>Se<sub>3</sub> with a layered structure in a bulk single-crystal form was used for the measurements.

### 2.2. Characterization

The X-ray diffraction was performed on all six indium(III) and gallium(III) chalcogenides to identify the phase composition. X-ray diffraction patterns (Figure 1) show the single-phase composition of the synthesized chalcogenides.

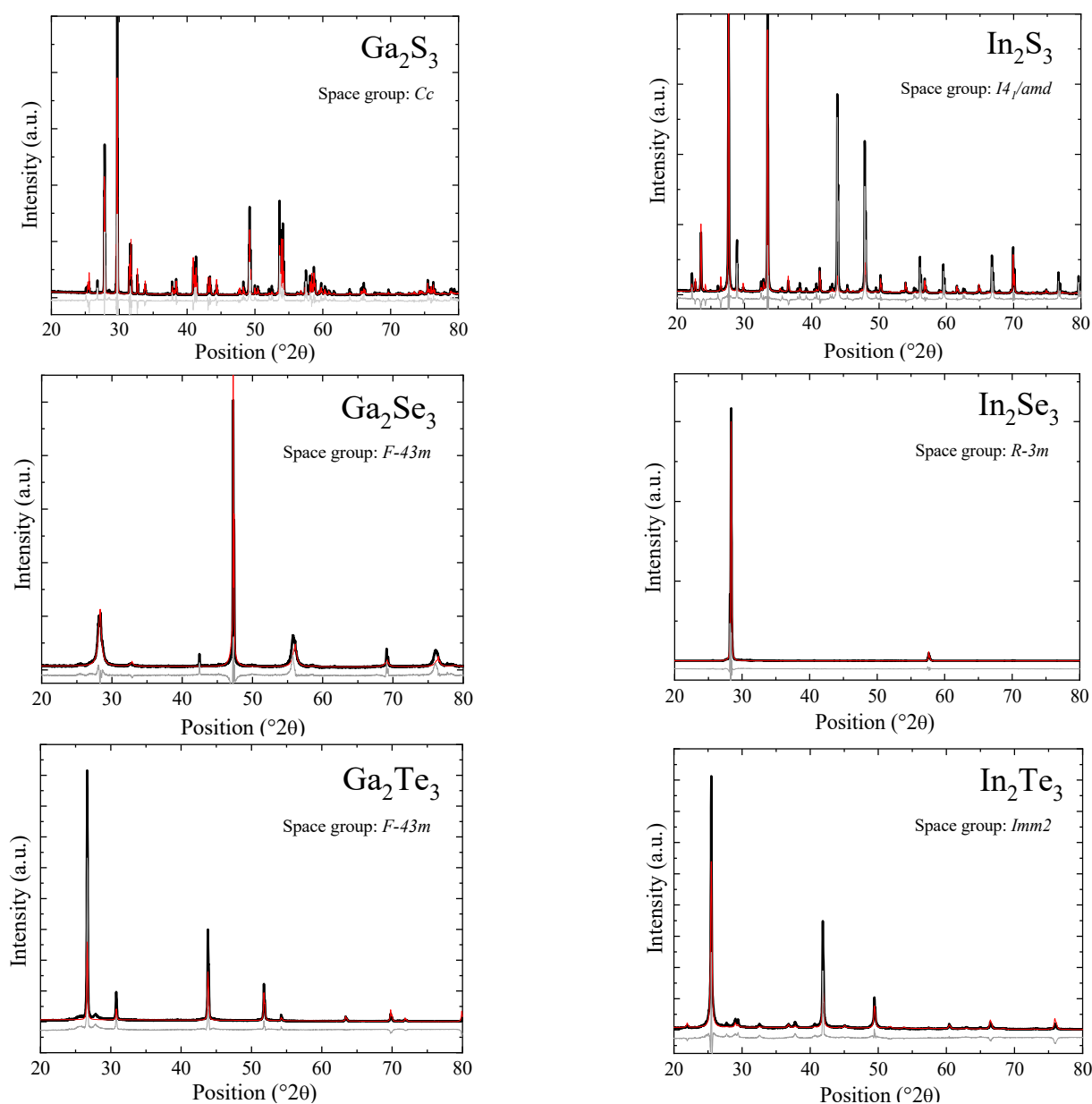


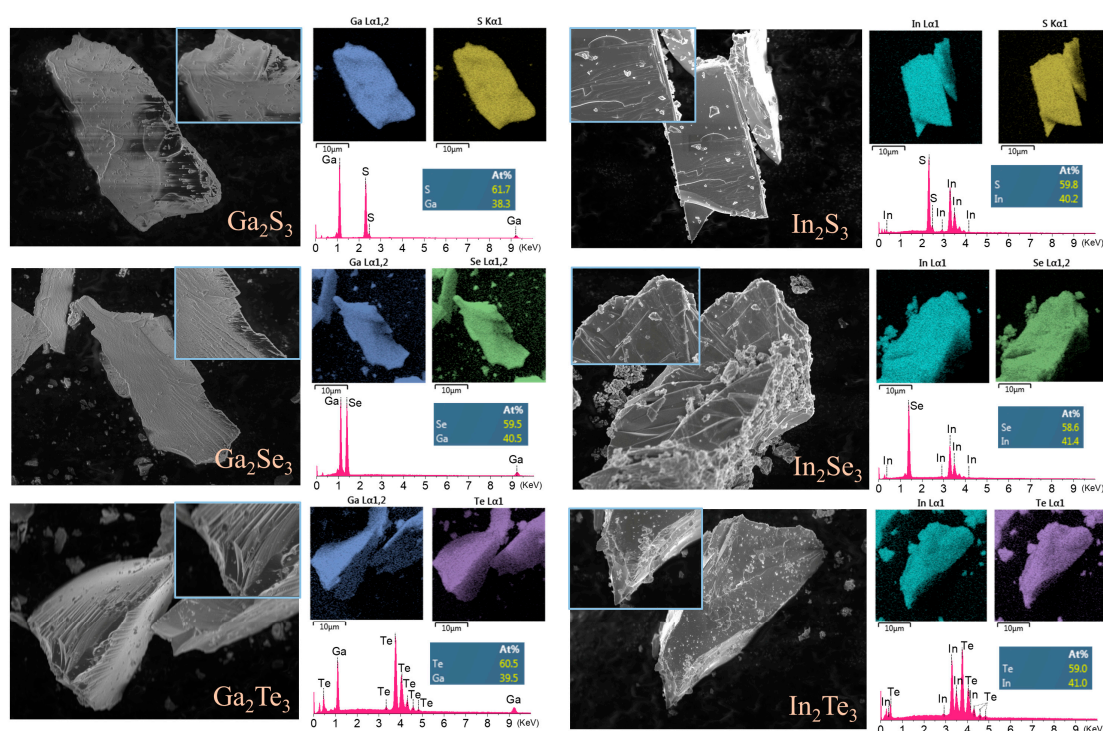
**Figure 1.** X-ray diffraction patterns of indium and gallium chalcogenides (black) and their Rietveld refinement (calculated profile—red, difference profile—gray).

Indium sulfide crystallized in a tetragonal structure (space group  $I4_1/amd$ ). Indium selenide reveals a rhombohedral layered structure (space group  $R-3mH$ ), and the X-ray diffractogram exhibits a preferential orientation due to the layered structure. Gallium telluride and gallium selenide crystallize in a cubic structure (space group  $F-43m$ ) derived from the zinc blende type with vacancies disordered on the cation sublattice, while gallium sulfide and indium telluride represent, respectively, ordered monoclinic (space group  $Cc$ ) and orthorhombic ( $Im-2$ ) forms of the metal-deficient zinc blende structure. The structure parameters obtained using Rietveld refinement (Topas program) based on the space groups given above are given in Table 1.

**Table 1.** Lattice parameters of  $\text{Ga}_2\text{S}_3$ ,  $\text{Ga}_2\text{Se}_3$ ,  $\text{Ga}_2\text{Te}_3$ ,  $\text{In}_2\text{S}_3$ ,  $\text{In}_2\text{Se}_3$ , and  $\text{In}_2\text{Te}_3$  as obtained with Rietveld refinement of the recorded X-ray diffraction patterns using Topas program.

	$\text{Ga}_2\text{S}_3$	$\text{Ga}_2\text{Se}_3$	$\text{Ga}_2\text{Te}_3$	$\text{In}_2\text{S}_3$	$\text{In}_2\text{Se}_3$	$\text{In}_2\text{Te}_3$
Space group	Cc	<i>F-43m</i>	<i>F-43m</i>	<i>I4<sub>1</sub>/amd</i>	<i>R-3mH</i>	<i>Imm2</i>
Lattice parameters/Å	a = 11.1172 b = °6.4041 c = °7.0305 β = °121.19	a = 5.4235	a = 5.903	a = 7.617 c = 32.32	a = °3.978 c = 28.99	a = 13.083 b = °4.361 c = °6.168

The morphologies and chemical compositions of the synthesized indium(III) and gallium(III) chalcogenides were meticulously characterized using scanning electron microscopy (SEM, Tescan MAIA 3, Dortmund, Germany) coupled with energy-dispersive X-ray spectroscopy (EDS, Oxford Instruments, Abingdon-on-Thames, UK), as shown in Figure 2.

**Figure 2.** SEM images, elemental mappings, and EDS spectrum of prepared indium and gallium chalcogenides.

The SEM analysis revealed a distinctive layered stacking morphology present in all chalcogenide compounds, encompassing both gallium and indium variants:  $\text{Ga}_2\text{S}_3$ ,  $\text{Ga}_2\text{Se}_3$ ,  $\text{Ga}_2\text{Te}_3$ , as well as  $\text{In}_2\text{S}_3$ ,  $\text{In}_2\text{Se}_3$ , and  $\text{In}_2\text{Te}_3$ . Elemental mapping through EDS showcased a uniform distribution of constituent elements within the material matrix. Additionally, the observed elemental ratios closely aligned with the stoichiometric 2:3 ratio for gallium/indium to chalcogen, highlighting the precision of the synthetic approach. These findings affirm the successful formation of the target compounds, emphasizing their desired chemical composition and structural integrity.

The composition of all six materials was further confirmed with X-ray photoelectron spectroscopy (XPS) using a SPECS spectrometer equipped with a monochromatic  $\text{Al K}\alpha$  X-ray source (1486.7 eV) and a hemispherical electron analyzer, Phoibos 150. Figure 3 displays high-resolution spectra of Ga-2p and In-3d core regions of the materials. In the gallium-containing chalcogenides, two broad signals are evident—the Ga-2p<sub>3/2</sub> and Ga-2p<sub>1/2</sub> core levels are situated at approximately 1118 and 1145 eV, respectively, and could be fitted with

a single component each. Similarly, the spectra of the indium-based chalcogenides exhibit two broad signals—the In- $3d_{5/2}$  and In- $3d_{3/2}$  core levels are located at approximately 453 and 445 eV, respectively. Like the gallium derivatives, these could be fitted with a single component each. The binding energy values correspond to the expected values for this class of compounds.

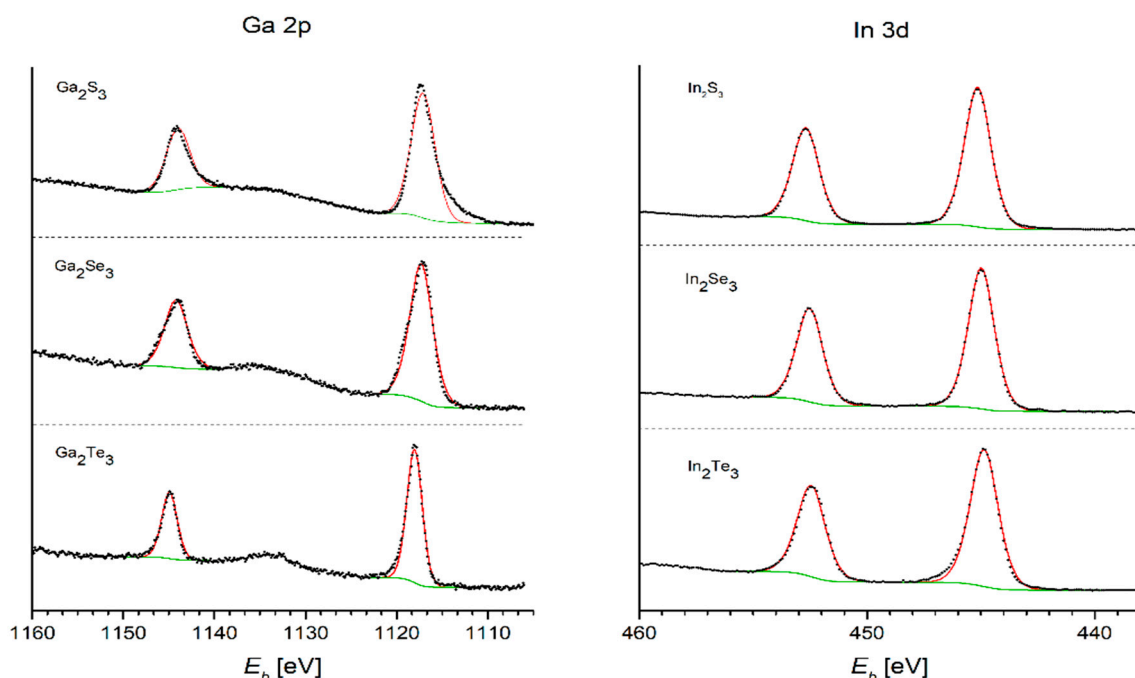


**Figure 3.** The Ga- $2p$  (left) and In- $3d$  (right) core regions of the XPS spectra of the chalcogenides of interest. Black dots represent the acquired data, the green curves the applied background correction, the red curves the fits.

Similarly, the spectra of the core regions of the chalcogenides ( $S-2p$ ,  $Se-3d$ , and  $Te-3d$ , respectively) show the characteristics expected for this type of compounds (Figures S1–S3). The  $S-2p$  regions of both sulfides show a single signal located at  $\sim 162$  eV, with well-resolved  $S-2p_{1/2}$  and  $S-2p_{3/2}$  components in the case of  $In_2S_3$ . Both selenides ( $In_2Se_3$  as well as  $Ga_2Se_3$ ) show one broad signal in the  $Se-3d$  region at  $\sim 54$  eV that could be fitted with a single pair of the  $3d_{3/2}$  and  $3d_{5/2}$  components each. There are two well-resolved signals in the spectra of the  $Te-3d$  core region of both,  $In_2Te_3$  as well as  $Ga_2Te_3$ , located at  $\sim 573$  eV ( $3d_{5/2}$ ) and  $\sim 583$  eV ( $3d_{3/2}$ ), respectively. Each of the signals could be fitted with a single component.

The Raman spectra of all the chalcogenides were recorded using a 532 nm Nd laser with low incident power and a  $20\times$  objective lens. There are two main resonance peaks in the spectrum of  $Ga_2S_3$  (Figure 4) identified at  $235$  and  $389$   $cm^{-1}$ , assigned to the  $A_1$  and  $F_2$  modes, respectively [13], accompanied with several lower intensity peaks in the regions  $70$ – $170$  and  $300$ – $360$   $cm^{-1}$ . The spectra of the other two gallium(III) chalcogenides,  $Ga_2Se_3$  and  $Ga_2Te_3$ , contain no sharp peaks but not-well-resolved broad signals with the maximum intensities at  $157$ ,  $243$ , and  $290$   $cm^{-1}$  for the selenide and  $58$  and  $118$   $cm^{-1}$  for the telluride. The shape and quality of these spectra correspond to the data reported [14,15]. In the Raman spectrum of  $In_2S_3$ , there are several well-resolved peaks that could be assigned to the  $A_{1g}$  modes ( $245$ ,  $309$ , and  $369$   $cm^{-1}$ ),  $E_g$  mode ( $269$   $cm^{-1}$ ), and  $F_{2g}$  modes ( $117$ ,  $183$ , and  $326$   $cm^{-1}$ ) [16]. Similarly to the heavier gallium chalcogenides, the spectra of indium selenide and telluride are also less resolved than the spectrum of the sulfide (Figure 4). In the spectrum of  $In_2Se_3$ , there are three major signals at  $106$ ,  $181$ , and  $200$   $cm^{-1}$  assigned to the  $A_1$  modes [17]. The spectrum of  $In_2Te_3$  corresponds to the only reported spectrum of this compound [18], with four main features at  $63$ ,  $105$ ,  $121$ , and  $140$   $cm^{-1}$ .

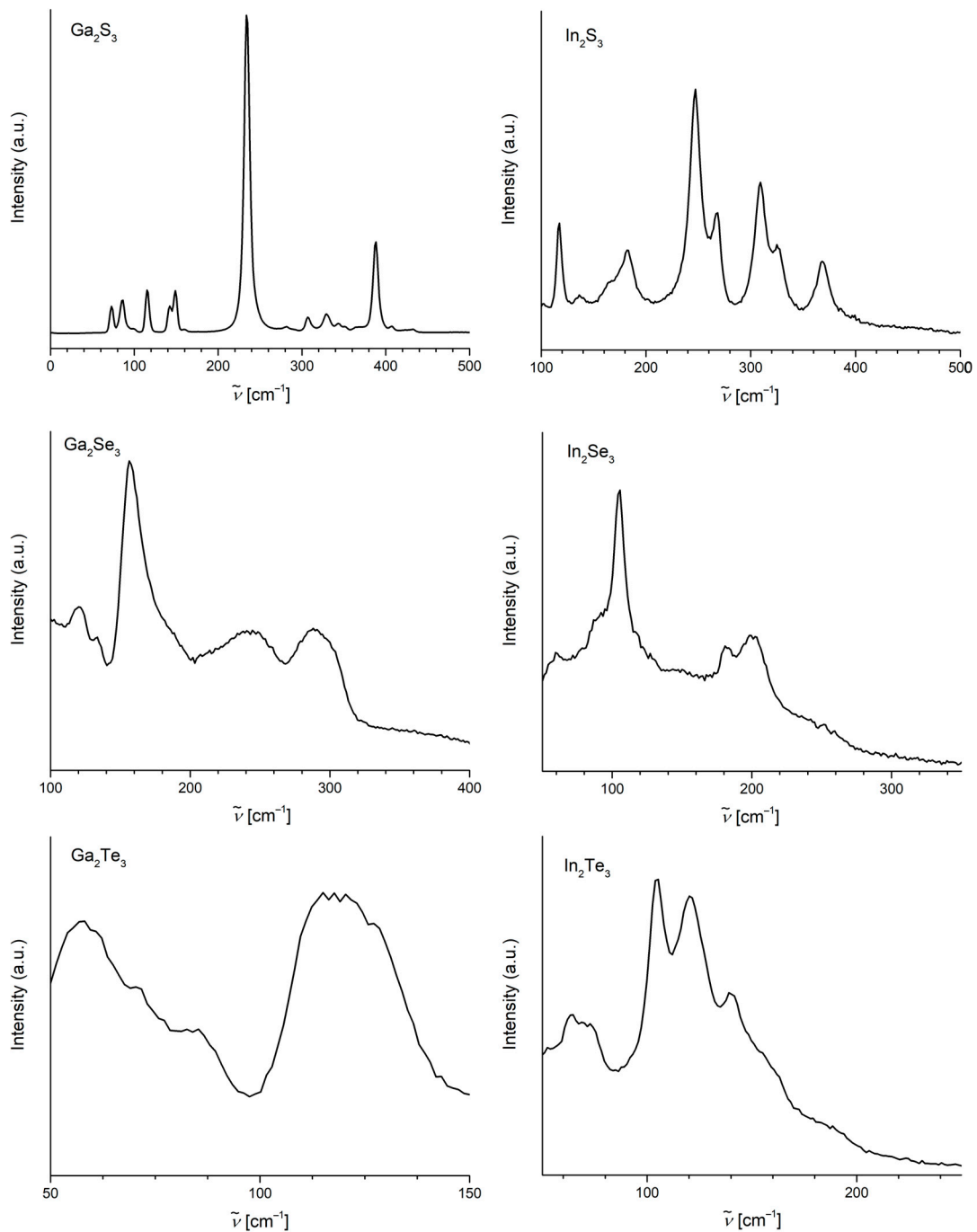


**Figure 4.** Raman spectra of the chalcogenides.

### 2.3. Calorimetric Measurements

A Tian–Calvet-type calorimeter (SETARAM  $\mu$ DSC IIIa, Caluire, France) was used to determine the heat capacity in the temperature range 258–358 K. The heat capacities were obtained using a continuous method [19]. A three-step procedure was used, where the reference cell was always empty, while the measuring cell was empty, filled with a reference substance (synthetic sapphire, NIST standard reference material No. 720, Gaithersburg, MD, USA) and a sample. The combined expanded uncertainty of the heat capacity measurements (confidence level 0.95) is estimated to be  $U_c(C_{pm}) = 0.01 C_{pm}$  [20].

Physical Property Measurement System (PPMS) Model 6000 EverCool II (Quantum Design, San Diego, CA, USA), equipped with a heat capacity module ( $^4\text{He}$ ,  $T_{\min} = 1.8$  K), was used for the heat capacity measurements in the low-temperature region (2–300 K).

The measurements were performed using the relaxation method under a high vacuum (pressure of  $10^{-2} \pm 10^{-3}$  Pa) to avoid heat loss through the exchange gas. The samples were wrapped in a copper foil and pressed into a pellet (with the exception of  $\text{In}_2\text{Se}_3$ , which was in the form of a monocrystal). These pellets were then mounted on a calorimeter platform using cryogenic grease, Apiezon N (supplied by the calorimeter manufacturer Quantum Design) [21]. The sample heat capacity was obtained as the difference between two data sets resulting from the sample run and the addenda (a blank sample holder with Apiezon N) performed under identical conditions. The uncertainty of heat capacity obtained using PPMS was recently investigated in our laboratory [21,22]. Based on tests with several compounds [21,22], the combined expanded uncertainty (0.95 level of confidence) of the heat capacity measurements is estimated to be 10 percent below 10 K, 3 percent in the temperature range of 10–40 K, and 2 percent in the temperature range of 40–300 K. To enhance the accuracy of the PPMS data, the results from this calorimeter were slightly adjusted to align with the results from the more accurate SETARAM  $\mu\text{DSC IIIa}$ , following common practice [23].

The following equation proposed by Archer [24] was used to describe temperature dependence of heat capacity in a wide temperature range (including literature heat capacities obtained using adiabatic calorimetry and data obtained using Quantum Design PPMS):

$$C_{pm}^o / C_{pm}^{\text{ref}} = \left( \frac{T}{T^{\text{ref}} f(T) + bT} \right)^3 \quad (1)$$

where  $T^{\text{ref}} = 1$  K and  $C_{pm}^{\text{ref}} = 1 \text{ J}\cdot\text{K}^{-1}\cdot\text{mol}^{-1}$  and

$$f(T) = a_i(T - T_i)^3 + b_i(T - T_i)^2 + c_i(T - T_i) + d_i \quad (2)$$

where only one parameter,  $d_i$ , needs to be optimized for each temperature interval, while the values of the other three are determined using the continuity and smoothness constraints of the resulting temperature dependence. The parameter  $b$  is determined from the slope of  $f(T)$  at temperatures greater than 70 K [24].

#### 2.4. DFT Calculations

The electronic structure calculations were performed within the VASP 5.4 program as implemented in the MedeA 3.6 software package using a Projector Augmented Waves method (PAW) [25] and a Generalized Gradient Approximation (GGA) with a PBE parametrization scheme [26]. The integration was performed using a tetrahedron method with Blöchl corrections on a mesh of  $k$ -points within the first Brillouin zone with a density of  $0.25 \text{ \AA}^{-1}$ . The structure parameters of group 13 sesqui-chalcogenides given in Table 1 were considered, with the exception of  $\text{Ga}_2\text{Se}_3$  whose ordered form with monoclinic  $Cc$  symmetry (analogous to  $\text{Ga}_2\text{S}_3$ ) was adopted. The obtained total energies were referred to the constituent elements in their ground state structure forms to evaluate the respective enthalpies of formation.

### 3. Results

#### 3.1. Heat Capacities

The experimental heat capacities obtained in this work using SETARAM  $\mu\text{DSC IIIa}$  and Quantum Design PPMS are listed in the Supplementary Materials (SMs) in Tables S1–S12. The available literature data on solid-phase heat capacities are summarized in Table 2. Selected experimental data from Table 2 (written in bold) were fitted to Equations (1) and (2), the parameters of which are listed in Table 3.

**Table 2.** Overview of the Literature Crystal Heat Capacities of Ga<sub>2</sub>S<sub>3</sub>, Ga<sub>2</sub>Se<sub>3</sub>, Ga<sub>2</sub>Te<sub>3</sub>, In<sub>2</sub>S<sub>3</sub>, In<sub>2</sub>Se<sub>3</sub>, and In<sub>2</sub>Te<sub>3</sub>.

Reference	$N^a$	$(T_{\min} - T_{\max})/K$	$u_r(C_{pm})/\%^b$	Method
Ga <sub>2</sub> S <sub>3</sub>				
Knacke et al. [27]	S <sup>c</sup>	298–1213	nosp.	nosp.
<b>This work</b>	<b>18</b>	<b>271–353</b>	<b>1.0</b>	<b>Tian–Calvet</b>
<b>This work</b>	<b>126</b>	<b>2–302</b>	<b>d</b>	<b>Relaxation</b>
Ga <sub>2</sub> Se <sub>3</sub>				
Knacke et al. [27]	S <sup>c</sup>	298–1278	nosp.	nosp.
Tyurin et al. [28]	101	15–324	0.2	Adiabatic
<b>This work</b>	<b>19</b>	<b>266–353</b>	<b>1.0</b>	<b>Tian–Calvet</b>
<b>This work</b>	<b>125</b>	<b>2–302</b>	<b>d</b>	<b>Relaxation</b>
Ga <sub>2</sub> Te <sub>3</sub>				
Knacke et al. [27]	S <sup>c</sup>	298–1063	nosp.	nosp.
Tyurin et al. [29]	134	9–310	0.2	Adiabatic
<b>This work</b>	<b>19</b>	<b>271–353</b>	<b>1.0</b>	<b>Tian–Calvet</b>
<b>This work</b>	<b>132</b>	<b>2–303</b>	<b>d</b>	<b>Relaxation</b>
In <sub>2</sub> S <sub>3</sub>				
Knacke et al. [27]	S <sup>c</sup>	298–660	nosp.	nosp.
<b>This work</b>	<b>14</b>	<b>262–323</b>	<b>1.0</b>	<b>Tian–Calvet</b>
<b>This work</b>	<b>125</b>	<b>2–302</b>	<b>d</b>	<b>Relaxation</b>
In <sub>2</sub> Se <sub>3</sub>				
Knacke et al. [27]	S <sup>c</sup>	298–470	nosp.	nosp.
Koshchenko et al. [30]	99	4–304	0.5	Adiabatic
Boehnke et al. [31]	138	6–285	0.1	Adiabatic
Mills [32]	5	298–486	0.5	DSC
<b>This work</b>	<b>19</b>	<b>262–350</b>	<b>1.0</b>	<b>Tian–Calvet</b>
<b>This work</b>	<b>104</b>	<b>2–226</b>	<b>d</b>	<b>Relaxation</b>
This work	22	232–302	d	Relaxation
In <sub>2</sub> Te <sub>3</sub>				
Knacke et al. [27]	S <sup>c</sup>	298–898	nosp.	nosp.
Zlomanov et al. [33]	75	5–313	0.2	Adiabatic
<b>This work</b>	<b>19</b>	<b>262–348</b>	<b>1.0</b>	<b>Tian–Calvet</b>
<b>This work</b>	<b>126</b>	<b>2–303</b>	<b>d</b>	<b>Relaxation</b>

<sup>a</sup>  $N$  = number of data points. <sup>b</sup>  $u_r(C_{pm})$  stands for relative uncertainty in heat capacity as stated by the authors. <sup>c</sup> S stands for smoothed data (given in the form of an equation); <sup>d</sup> the combined expanded uncertainty of heat capacity with 0.95 level of confidence ( $k = 2$ ) of PPMS using thermal relaxation measurement technique is  $U_c(C_{pm}) = 0.1 C_{pm}$  below 10 K;  $U_c(C_{pm}) = 0.03 C_{pm}$  in temperature range 10 to 40 K;  $U_c(C_{pm}) = 0.02 C_{pm}$  in temperature range 40 to 300 K.

The thermodynamic functions obtained using Equations (1) and (2) are tabulated at 298.15 K in Table 4, and at other temperatures in Tables S13–S18 in the SM, and shown in Figure 5.

**Table 3.** Parameters of Equations (1) and (2) for Crystal Heat Capacities in  $\text{J}\cdot\text{K}^{-1}\text{ mol}^{-1}$ .

$a_i$	$b_i$	$c_i$	$d_i$	$T_i/\text{K}$	$T_{i,\text{max}}/\text{K}$	$N^a$	$s_r^b$
$\text{Ga}_2\text{S}_3$				$b = 0.18$			
$1.10116 \times 10^{-2}$	$-2.03631 \times 10^{-1}$	$9.61860 \times 10^{-1}$	$1.23920 \times 10^1$	0	5	14	0.93
$2.81063 \times 10^{-3}$	$-3.84571 \times 10^{-2}$	$-2.48579 \times 10^{-1}$	$1.34870 \times 10^1$	5	12	8	1.17
$-6.13516 \times 10^{-4}$	$2.05661 \times 10^{-2}$	$-3.73816 \times 10^{-1}$	$1.08266 \times 10^1$	12	20	8	2.74
$-6.72147 \times 10^{-5}$	$5.84174 \times 10^{-3}$	$-1.62553 \times 10^{-1}$	8.83815	20	50	17	1.09
$1.43753 \times 10^{-6}$	$-2.07582 \times 10^{-4}$	$6.47156 \times 10^{-3}$	7.40433	50	100	19	0.56
$1.74864 \times 10^{-7}$	$8.04748 \times 10^{-6}$	$-3.50518 \times 10^{-3}$	7.38864	100	200	30	0.40
$-1.34810 \times 10^{-7}$	$6.05065 \times 10^{-5}$	$3.35023 \times 10^{-3}$	7.29346	200	353	48	0.36
$\text{Ga}_2\text{Se}_3$				$b = 0.19$			
$5.69538 \times 10^{-2}$	$-8.73244 \times 10^{-1}$	4.22755	2.28158	0	5	10	1.60
$1.75173 \times 10^{-3}$	$-1.89368 \times 10^{-2}$	$-2.33356 \times 10^{-1}$	8.70745	5	12	10	1.00
$-6.36373 \times 10^{-4}$	$1.78496 \times 10^{-2}$	$-2.40966 \times 10^{-1}$	6.74691	12	20	8	1.07
$-3.14760 \times 10^{-5}$	$2.57666 \times 10^{-3}$	$-7.75553 \times 10^{-2}$	5.63574	20	50	16	0.77
$2.57153 \times 10^{-6}$	$-2.56181 \times 10^{-4}$	$-7.94088 \times 10^{-3}$	4.77822	50	100	19	0.42
$-3.97876 \times 10^{-7}$	$1.29549 \times 10^{-4}$	$-1.42725 \times 10^{-2}$	4.06217	100	200	30	0.26
$7.82412 \times 10^{-8}$	$1.01860 \times 10^{-5}$	$-2.99051 \times 10^{-4}$	3.53252	200	353	37	0.18
$\text{Ga}_2\text{Te}_3$				$b = 0.19$			
$1.11589 \times 10^{-2}$	$-1.47396 \times 10^{-1}$	$2.08914 \times 10^{-1}$	7.96519	0	5	14	0.90
$-1.70943 \times 10^{-4}$	$1.99869 \times 10^{-2}$	$-4.28133 \times 10^{-1}$	6.71971	5	12	8	1.70
$-6.39490 \times 10^{-4}$	$1.63972 \times 10^{-2}$	$-1.73444 \times 10^{-1}$	4.64351	12	20	8	2.18
$-1.32927 \times 10^{-5}$	$1.04939 \times 10^{-3}$	$-3.38717 \times 10^{-2}$	3.97796	20	50	16	0.74
$1.62523 \times 10^{-6}$	$-1.46950 \times 10^{-4}$	$-6.79852 \times 10^{-3}$	3.54735	50	100	20	0.56
$-3.13065 \times 10^{-7}$	$9.68342 \times 10^{-5}$	$-9.30432 \times 10^{-3}$	3.04321	100	200	30	0.29
$1.02416 \times 10^{-7}$	$2.91463 \times 10^{-6}$	$6.70564 \times 10^{-4}$	2.76805	200	353	34	0.18
$\text{In}_2\text{S}_3$				$b = 0.19$			
$2.79528 \times 10^{-2}$	$-3.99655 \times 10^{-1}$	1.29063	$1.00431 \times 10^1$	0	5	14	1.78
$4.94311 \times 10^{-4}$	$1.96370 \times 10^{-2}$	$-6.09463 \times 10^{-1}$	9.99897	5	12	8	3.11
$-1.21050 \times 10^{-3}$	$3.00175 \times 10^{-2}$	$-2.61881 \times 10^{-1}$	6.86449	12	20	8	2.61
$-1.61253 \times 10^{-5}$	$9.65519 \times 10^{-4}$	$-1.40172 \times 10^{-2}$	6.07079	20	50	17	0.69
$4.10646 \times 10^{-6}$	$-4.85758 \times 10^{-4}$	$3.75668 \times 10^{-4}$	6.08385	50	100	19	0.48
$-3.81795 \times 10^{-7}$	$1.30212 \times 10^{-4}$	$-1.74016 \times 10^{-2}$	5.40155	100	200	30	0.29
$2.88444 \times 10^{-7}$	$1.56732 \times 10^{-5}$	$-2.81313 \times 10^{-3}$	4.58171	200	323	38	0.33
$\text{In}_2\text{Se}_3$				$b = 0.18$			
$1.51705 \times 10^{-2}$	$-1.95861 \times 10^{-1}$	$3.7698 \times 10^{-1}$	8.19467	0	5	14	0.94
$-8.54900 \times 10^{-4}$	$3.16966 \times 10^{-2}$	$-4.43834 \times 10^{-1}$	7.07940	5	12	14	3.24
$-5.67811 \times 10^{-4}$	$1.37437 \times 10^{-2}$	$-1.25752 \times 10^{-1}$	5.23246	12	20	18	1.71
$-3.28446 \times 10^{-7}$	$1.16225 \times 10^{-4}$	$-1.48729 \times 10^{-2}$	4.81532	20	50	41	1.03
$9.00517 \times 10^{-8}$	$8.66649 \times 10^{-5}$	$-8.78617 \times 10^{-3}$	4.46487	50	100	66	0.59
$-3.04634 \times 10^{-7}$	$1.00173 \times 10^{-4}$	$5.55706 \times 10^{-4}$	4.25348	100	200	100	0.31
$-5.99553 \times 10^{-8}$	$8.78254 \times 10^{-6}$	$1.14512 \times 10^{-2}$	5.00614	200	350	56	0.20
$\text{In}_2\text{Te}_3$				$b = 0.19$			
$1.46034 \times 10^{-2}$	$-1.76452 \times 10^{-1}$	$1.85958 \times 10^{-1}$	6.88854	0	5	14	0.33
$-1.45817 \times 10^{-3}$	$4.25984 \times 10^{-2}$	$-4.83311 \times 10^{-1}$	5.23244	5	12	8	1.60
$-5.00450 \times 10^{-4}$	$1.19768 \times 10^{-2}$	$-1.01284 \times 10^{-1}$	3.43644	12	20	8	2.36
$-9.09745 \times 10^{-8}$	$-3.39669 \times 10^{-5}$	$-5.74150 \times 10^{-3}$	3.13645	20	50	16	0.87
$9.49425 \times 10^{-7}$	$-4.21546 \times 10^{-5}$	$-8.02514 \times 10^{-3}$	2.93118	50	100	20	0.45
$-3.69997 \times 10^{-7}$	$1.00259 \times 10^{-4}$	$-5.11991 \times 10^{-3}$	2.54321	100	200	30	0.23
$9.21853 \times 10^{-8}$	$-1.07400 \times 10^{-5}$	$3.83202 \times 10^{-3}$	2.66382	200	348	49	0.28

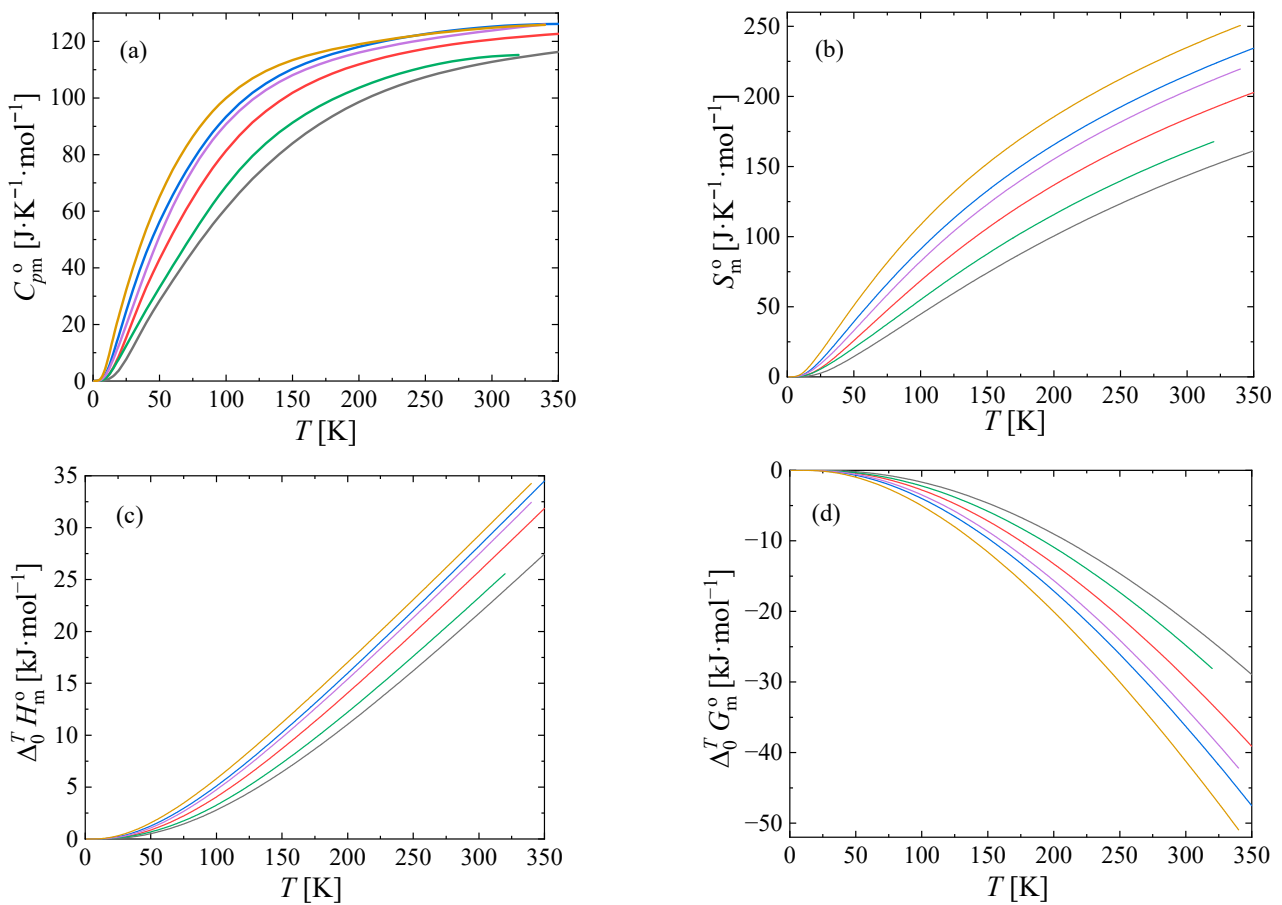
<sup>a</sup>  $N$  stands for number of experimental data points in given temperature interval used for correlation.

<sup>b</sup>  $s_r = 100 \left\{ \sum_{i=1}^n \left[ \left( C_{pm}^{\text{exp}} - C_{pm}^{\text{calc}} \right) / C_{pm}^{\text{calc}} \right]^2 / (N - m) \right\}^{1/2}$ , where  $C_{pm}^{\text{exp}}$  and  $C_{pm}^{\text{calc}}$  are the experimental and calculated (Equations (1) and (2)) heat capacity,  $N$  is the number of fitted data points, and  $m$  is the number of independent adjustable parameters.

**Table 4.** Standard Thermodynamic Functions of Ga(III) and In(III) chalcogenides derived from heat capacity measurements and the calculated enthalpies of formation at  $T = 298.15$  K and  $p = 0.1$  MPa <sup>a</sup>.

	$C_{pm}^{\circ}/\text{J}\cdot\text{K}^{-1}\cdot\text{mol}^{-1}$	$\Delta_f H^{\circ}/\text{kJ}\cdot\text{mol}^{-1}$	$S_m^{\circ}/\text{J}\cdot\text{K}^{-1}\cdot\text{mol}^{-1}$	$\Delta_0^T H_m^{\circ}/\text{kJ}\cdot\text{mol}^{-1}$	$\Delta_0^T G_m^{\circ}/\text{kJ}\cdot\text{mol}^{-1}$
Ga <sub>2</sub> S <sub>3</sub>	112.6	−353.5	142.8	21.51	−21.06
Ga <sub>2</sub> Se <sub>3</sub>	120.6	−299.9	183.2	25.54	−29.09
Ga <sub>2</sub> Te <sub>3</sub>	125.1	−140.7	214.2	27.97	−35.88
In <sub>2</sub> S <sub>3</sub>	114.6	−282.5	159.6	23.05	−24.53
In <sub>2</sub> Se <sub>3</sub>	123.8	−263.6	203.1	27.21	−33.36
In <sub>2</sub> Te <sub>3</sub>	124.7	−68.4	234.1	29.02	−40.78

<sup>a</sup> The combined expanded uncertainty of heat capacity  $U_c(C_{pm})$  as well as of all calculated thermodynamic values (with 0.95 level of confidence,  $k = 2$ ) is  $U_c(X) = 0.01 X$  in temperature range 260 to 340 K, where  $X$  represents the heat capacity or the thermodynamic property. Values are reported with one digit more than is justified by the experimental uncertainty to avoid round-off errors in calculations based on these results.

**Figure 5.** Standard molar thermodynamic functions at  $p = 0.1$  MPa. Ga<sub>2</sub>S<sub>3</sub> (black —), Ga<sub>2</sub>Se<sub>3</sub> (red —), Ga<sub>2</sub>Te<sub>3</sub> (blue —), In<sub>2</sub>S<sub>3</sub> (green —), In<sub>2</sub>Se<sub>3</sub> (purple —), In<sub>2</sub>Te<sub>3</sub> (olive —). (a) Isobaric heat capacity, (b) entropy, (c) enthalpy, and (d) Gibbs energy.

The experimental heat capacities for all studied chalcogenides are compared with the smoothed values obtained using Equations (1) and (2) in Figure 6. The deviations of the selected experimental data from the smoothed values generally do not exceed 2% (except for a few outliers, which are not considered in the correlation).

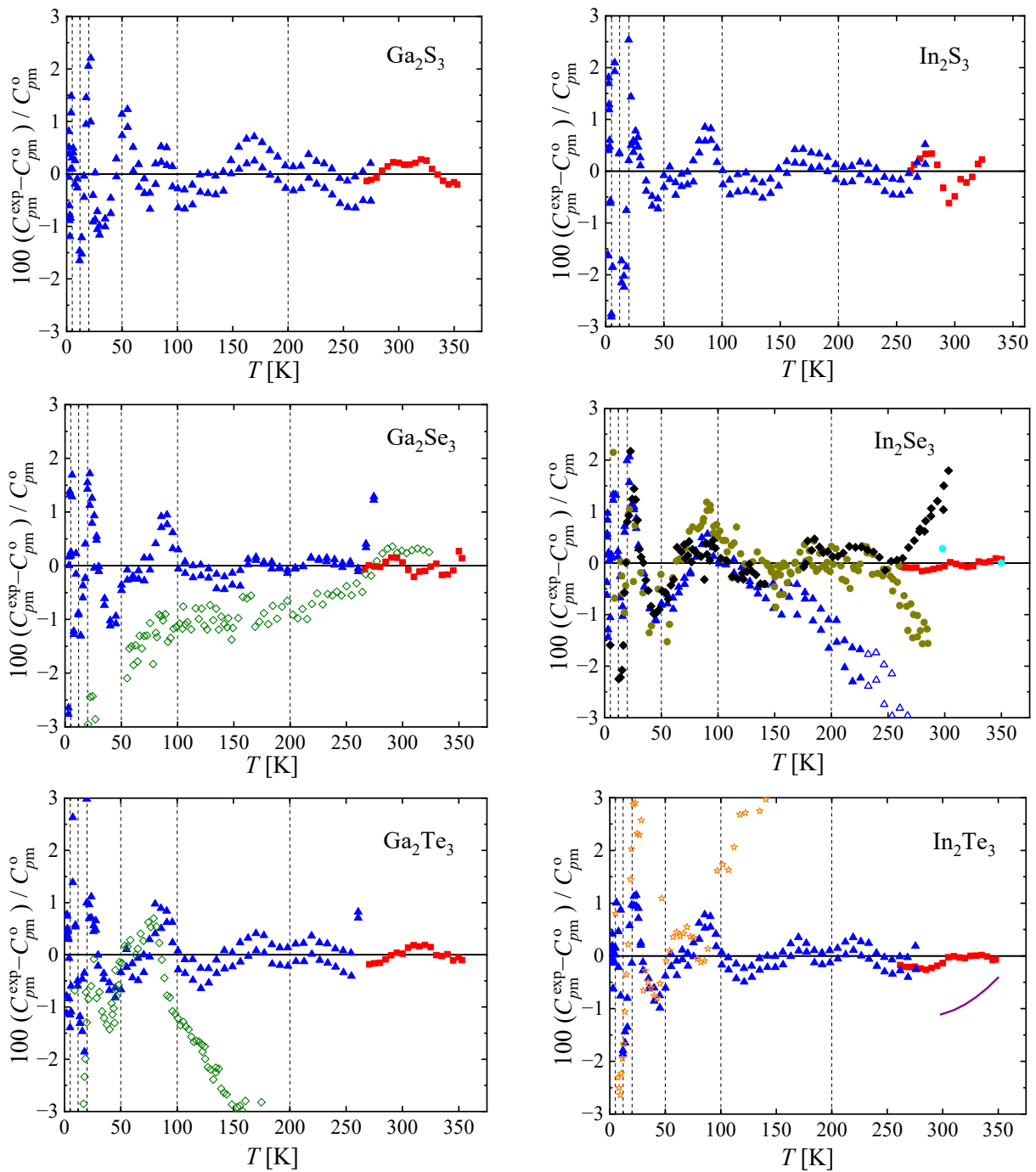


**Figure 6.** Relative deviations  $100(C_{pm}^{exp} - C_{pm}^o) / C_{pm}^o$  of individual experimental heat capacities  $C_{pm}^{exp}$  from values  $C_{pm}^o$  calculated by means of Equations (1) and (2) with parameters from Table 2. Red  $\blacksquare$ , this work (Tian–Calvet calorimetry); blue  $\blacktriangle$ , this work (relaxation calorimetry); purple  $—$ , Knacke et al. [27] (for all compounds except  $In_2Te_3$ , all data by Knacke et al. [27] are out of scale); green  $\blacklozenge$ , Tyurin et al. [28,29]; olive  $\bullet$ , Boehnke et al. [31]; black  $\blacklozenge$ , Koshchenko et al. [30]; orange  $\star$ , Zlomanov et al. [33]; cyan  $\bullet$ , Mills [32]. Vertical lines mark knot temperatures  $T_i$ . Data represented by filled symbols have been used to obtain parameters of Equations (1) and (2). Relaxation calorimetry data of this work for  $In_2Se_3$  above 230 K have been excluded due to low coupling.

### 3.2. Enthalpies of Formation

The total energies calculated in VASP with the PAW-GGA method were first recalculated to enthalpies of formation at  $T = 0$  K using the total energies of constituent elements

in their stable forms obtained with the same technique. As mentioned, the refined lattice parameters and atomic positions were used for the sesqui-chalcogenides (see Table 1, except for  $\text{Ga}_2\text{Se}_3$ , see Section 2.4), while the structure data of elements were adopted from the InfoMatica-ICSD database implemented in the MedeA software. The disordered structure of  $\text{Ga}_2\text{Se}_3$  of the zinc blende type was modeled in terms of a  $1 \times 1 \times 3$  supercell (12 formula units) with four vacant Ga positions  $(000, 1/2, 1/2, 1/3, 1/2, 0, 1/2, 1/2, 1/2, 2/3)$ . The enthalpies of formation at 0 K were further recalculated to cohesive energies using the enthalpies of vaporization of the constituent elements [34] and to the enthalpies of formation at a reference temperature of  $T = 298.15$  K (see Table 4) using the relative enthalpies 0→298 also given in Table 4 and the analogous relative enthalpies of elements [35].

#### 4. Discussion

The heat capacity of the studied chalcogenides was measured using the SETARAM  $\mu\text{DSC IIIa}$  and QuantumDesign PPMS calorimeters.  $\text{In}_2\text{Se}_3$  was measured in the form of a crystal, and the rest of the chalcogenides were grinded into powders and pressed into pellets covered with copper foil.

The results were compared with available literature (see Figure 6). A handbook by Knacke et al. [27] provides parameters for the heat capacity of these chalcogenides in a wide temperature range. These values differ significantly from our measurements (by 4 to 20%) with the exception of  $\text{In}_2\text{Te}_3$ , which agreed with our measurements within 1% in the range of overlap—from 300 to 350 K. The adiabatic heat capacity data by Tyurin et al. [28] agree with our measurements within 2% above 50 K in the case of  $\text{Ga}_2\text{Se}_3$ . Below 50 K, the difference increases to 20% at 15 K, the lowest point of Tyurin et al. [28]. Therefore, we decided not to include this data set in our correlation. On the other hand, adiabatic data by Tyurin et al. [29], Koschenko et al. [30], Boenke et al. [31], and Zlomanov et al. [33] are in good agreement with our measurements, with the exception of the tellurides ( $\text{Ga}_2\text{Te}_3$ ,  $\text{In}_2\text{Te}_3$ ), which deviate for temperatures above 100 K (with maximum deviation of 5% for  $\text{In}_2\text{Te}_3$  [33] and 9% for  $\text{Ga}_2\text{Te}_3$  [29]). However, at temperatures lower than 100 K, the agreement is also very good. The reason for the discrepancy observed above 100 K remains unclear and requires further elucidation.

The resulting heat capacities were fitted with the reverse spline function suggested by Archer et al. [24] and their comparison is shown in Figure 7.

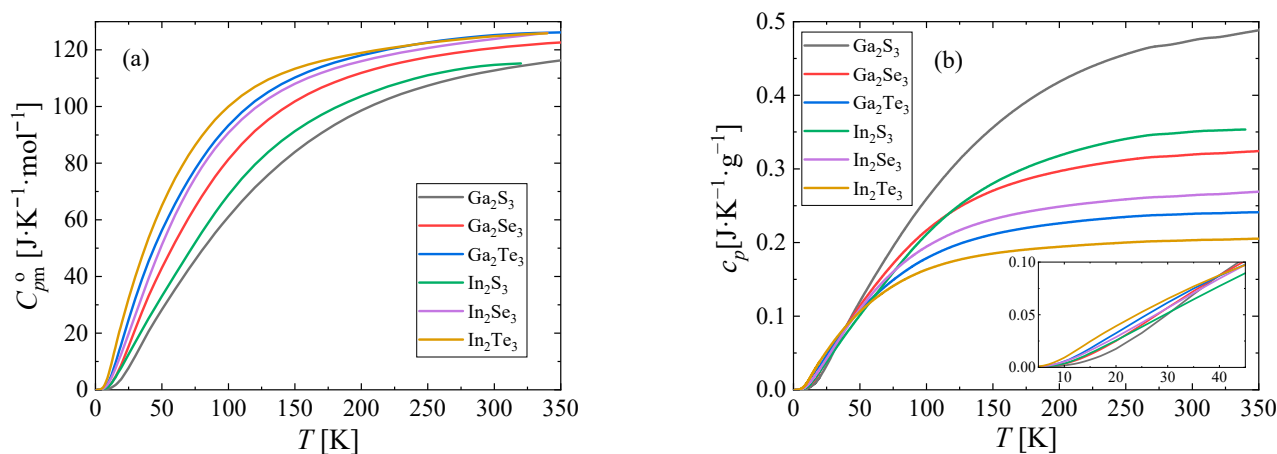


**Figure 7.** Heat capacity of Ga and In sesqui-chalcogenides studied in this work. (a) Molar, (b) specific.

As we can see in Figure 7a, the order of heat capacities (from highest to lowest) is  $\text{In}_2 > \text{Ga}_2$  and  $\text{Te}_3 > \text{Se}_3 > \text{S}_3$ . This clear trend is a manifestation of (i) increasing molar masses ( $M(\text{Ga}_2\text{S}_3) = 235.64$ ;  $M(\text{In}_2\text{Te}_3) = 612.44$ ) and (ii) softer force constants related to chemical bond weakening with increasing atomic size (due to less effective valence orbital overlap), both resulting in an enhanced phonon mode population at lower temperatures. In contrast, if we compare their specific heat capacities instead (Figure 7b), we obtain an

exact opposite order at ambient temperatures. Interestingly, the specific heat capacities cross over at about 40 K and at very low temperatures, the order of specific heat capacities being the same as for molar heat capacities (see the inset of Figure 7b).

The calculated enthalpies of formation at 298 K and cohesive energies at 0 K referred, respectively, to elements in their stable solid forms and to a noninteracting monoatomic gas are plotted in Figure 8a,b against the atomic number of chalcogen. In both cases, a decreasing stability with an increasing atomic number of group 16 as well as group 13 elements is apparently a result of decreasing strength of the covalent bond due to a less effective overlap of more diffused valence orbitals, which is also in line with the observed trend in molar heat capacities.

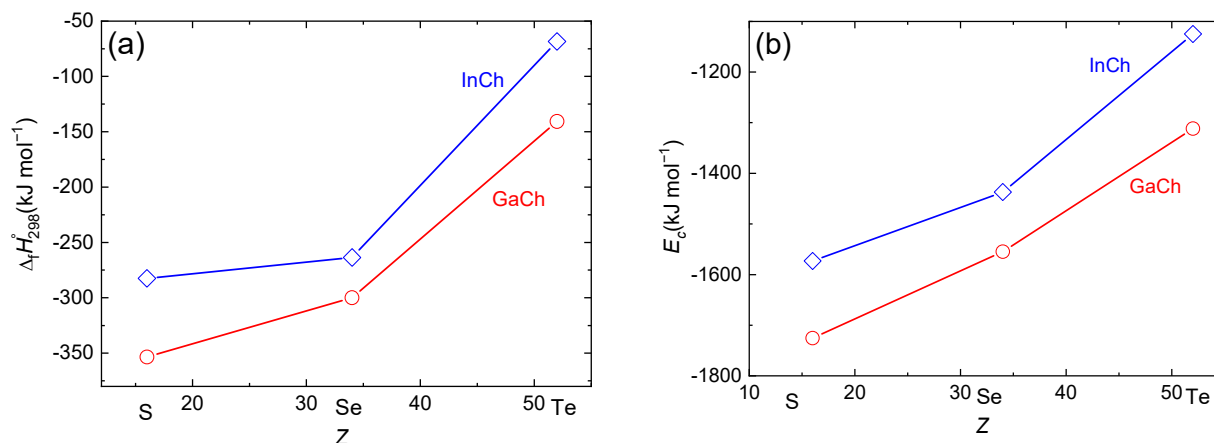


**Figure 8.** Enthalpies of formation (a) and cohesive energies (b) of Ga and In sesqui-chalcogenides evaluated from DFT calculations.

Although the calculated enthalpies of formation reveal an expected trend, their values are underestimated with respect to the data given in tables published by Knacke et al. [27]. However, the heat capacities of this work also do not agree well with Knacke et al. [27] so the two discrepancies might compensate each other in cases where the enthalpies of formation were assessed from high-temperature equilibrium data.

## 5. Conclusions

In this work, six sesqui-chalcogenides of indium and gallium were synthesized and characterized using XRD, SEM, XPS, and Raman spectroscopy. The heat capacity of gallium and indium sesqui-chalcogenides was determined by means of relaxation calorimetry (QuantumDesign PPMS) and Tian–Calvet calorimetry (SETARAM  $\mu$ DSC IIIa). Both techniques yielded consistent results comparable to available literature data obtained using adiabatic calorimetry. Moreover, the enthalpies of formation were assessed from DFT calculation of total energies. Experimental and theoretical data of this work, along with selected literature data, were used to derive standard thermodynamic data (enthalpy, entropy, Gibbs energy) in the temperature range from 0 K to 340 K.

**Supplementary Materials:** The following Supporting Information can be downloaded at: <https://www.mdpi.com/article/10.3390/ma17020361/s1>, X-ray photoelectron spectroscopy (XPS) results for the core regions of the chalcogenides (Figures S1–S3), Auxiliary properties describing the quality of PPMS measurement (Figures S4 and S5), Experimental heat capacity data obtained in this work (Tables S1–S12), Tabulated thermodynamic functions of studied sesqui-chalcogenides (Tables S13–S18).

**Author Contributions:** Conceptualization, Z.S. and D.S.; Data curation, V.P., J.P. and I.P.; Formal analysis, V.P.; Funding acquisition, Z.S.; Investigation, K.R., V.P., J.P., I.P., B.W. and D.S.; Methodology, K.R., Z.S. and D.S.; Resources, Z.S.; Supervision, D.S.; Visualization, V.P., J.P. and B.W.; Writing—

original draft, K.R. and V.P.; Writing—review and editing, K.R., Z.S. and D.S. All authors have read and agreed to the published version of the manuscript.

**Funding:** This work was supported by the project “The Energy Conversion and Storage”, funded as project No. CZ.02.01.01/00/22\_008/0004617 by Programme Johannes Amos Comenius, call Excellent Research. Z.S. was supported by ERC-CZ program (project LL2101) from Ministry of Education, Youth and Sports (MEYS) and used large infrastructure from project reg. No. CZ.02.1.01/0.0/0.0/15\_003/0000444 financed by the ERDF. Computational resources were provided by the e-INFRA CZ project (ID:90254), supported by the Ministry of Education, Youth and Sports of the Czech Republic.

**Institutional Review Board Statement:** Not applicable.

**Informed Consent Statement:** Not applicable.

**Data Availability Statement:** The data presented in this study are available in the Supplementary Materials.

**Conflicts of Interest:** The authors declare no conflicts of interest.

## References

1. Chhowalla, M.; Jena, D.; Zhang, H. Two-dimensional semiconductors for transistors. *Nat. Rev. Mater.* **2016**, *1*, 16052. [[CrossRef](#)]
2. Zhang, Y.; Rubio, A.; Lay, G.L. Emergent elemental two-dimensional materials beyond graphene. *J. Phys. D Appl. Phys.* **2017**, *50*, 053004. [[CrossRef](#)]
3. Ponraj, J.S.; Xu, Z.-Q.; Dhanabalan, S.C.; Mu, H.; Wang, Y.; Yuan, J.; Li, P.; Thakur, S.; Ashrafi, M.; McCoubrey, K.; et al. Photonics and optoelectronics of two-dimensional materials beyond graphene. *Nanotechnology* **2016**, *27*, 462001. [[CrossRef](#)] [[PubMed](#)]
4. Browning, R.; Kuperman, N.; Moon, B.; Solanki, R. Atomic Layer Growth of InSe and Sb<sub>2</sub>Se<sub>3</sub> Layered Semiconductors and Their Heterostructure. *Electronics* **2017**, *6*, 27. [[CrossRef](#)]
5. Tabernor, J.; Christian, P.; O'Brien, P. A general route to nanodimensional powders of indium chalcogenides. *J. Mater. Chem.* **2006**, *16*, 2082–2087. [[CrossRef](#)]
6. Mancini, A.M.; Micocci, G.; Rizzo, A. New materials for optoelectronic devices: Growth and characterization of indium and gallium chalcogenide layer compounds. *Mater. Chem. Phys.* **1983**, *9*, 29–54. [[CrossRef](#)]
7. Tan, C.K.Y.; Fu, W.; Loh, K.P. Polymorphism and Ferroelectricity in Indium(III) Selenide. *Chem. Rev.* **2023**, *123*, 8701–8717. [[CrossRef](#)]
8. Aksimentyeva, O.I.; Demchenko, P.Y.; Savchyn, V.P.; Balitskii, O.A. The chemical exfoliation phenomena in layered GaSe-polyaniline composite. *Nanoscale Res. Lett.* **2013**, *8*, 29. [[CrossRef](#)]
9. Mudd, G.W.; Svatek, S.A.; Ren, T.; Patanè, A.; Makarovskiy, O.; Eaves, L.; Beton, P.H.; Kovalyuk, Z.D.; Lashkarev, G.V.; Kudrynskiy, Z.R.; et al. Tuning the Bandgap of Exfoliated InSe Nanosheets by Quantum Confinement. *Adv. Mater.* **2013**, *25*, 5714–5718. [[CrossRef](#)]
10. Sfuncia, G.; Nicotra, G.; Giannazzo, F.; Pécz, B.; Gueorguiev, G.K.; Kakanakova-Georgieva, A. 2D graphitic-like gallium nitride and other structural selectivity in confinement at the graphene/SiC interface. *CrystEngComm* **2023**, *25*, 5810–5817. [[CrossRef](#)]
11. Sangiovanni, D.G.; Faccio, R.; Gueorguiev, G.K.; Kakanakova-Georgieva, A. Discovering atomistic pathways for supply of metal atoms from methyl-based precursors to graphene surface. *Phys. Chem. Chem. Phys.* **2023**, *25*, 829–837. [[CrossRef](#)]
12. Sedmidubský, D.; Sofer, Z.; Huber, Š.; Luxa, J.; Točík, R.; Mahnel, T.; Růžička, K. Chemical bonding and thermodynamic properties of gallium and indium monochalcogenides. *J. Chem. Thermodyn.* **2019**, *128*, 97–102. [[CrossRef](#)]
13. Julien, C.; Barnier, S.; Massot, M.; Pardo, M.P. Vibrational studies of solid solutions formed in the gallium-cadmium-sulphur system. *Mater. Res. Bull.* **1994**, *29*, 785–794. [[CrossRef](#)]
14. Krost, A.; Richter, W.; Zahn, D.R.T.; Hingerl, K.; Sitter, H. Chemical reaction at the ZnSe/GaAs interface detected by Raman spectroscopy. *Appl. Phys. Lett.* **1990**, *57*, 1981–1982. [[CrossRef](#)]
15. Halsall, M.P.; Wolverson, D.; Davies, J.J.; Lunn, B.; Ashenford, D.E. Ga<sub>2</sub>Te<sub>3</sub> and tellurium interfacial layers in ZnTe/GaSb heterostructures studied by Raman scattering. *Appl. Phys. Lett.* **1992**, *60*, 2129–2131. [[CrossRef](#)]
16. Tao, H.; Mao, S.; Dong, G.; Xiao, H.; Zhao, X. Raman scattering studies of the Ge–In sulfide glasses. *Solid State Commun.* **2006**, *137*, 408–412. [[CrossRef](#)]
17. Lewandowska, R.; Bacewicz, R.; Filipowicz, J.; Paszkowicz, W. Raman scattering in  $\alpha$ -In<sub>2</sub>Se<sub>3</sub> crystals. *Mater. Res. Bull.* **2001**, *36*, 2577–2583. [[CrossRef](#)]
18. Zahn, D.R.T.; Mackey, K.J.; Williams, R.H.; Münder, H.; Geurts, J.; Richter, W. Formation of interfacial layers in InSb–CdTe heterostructures studied by Raman scattering. *Appl. Phys. Lett.* **1987**, *50*, 742–744. [[CrossRef](#)]
19. Höhne, G.W.H.; Hemminger, W.F.; Flammersheim, H.-J. *Differential Scanning Calorimetry*, 2nd ed.; Springer: Berlin/Heidelberg, Germany, 2003.
20. Štejfa, V.; Fulem, M.; Růžička, K.; Červinka, C. Thermodynamic study of selected monoterpenes III. *J. Chem. Thermodyn.* **2014**, *79*, 280–289. [[CrossRef](#)]

21. Pokorný, V.; Štejfa, V.; Havlín, J.; Fulem, M.; Růžička, K. Heat Capacities of L-Cysteine, L-Serine, L-Threonine, L-Lysine, and L-Methionine. *Molecules* **2023**, *28*, 451. [[CrossRef](#)]
22. Mahnel, T.; Pokorný, V.; Fulem, M.; Sedmidubský, D.; Růžička, K. Measurement of low-temperature heat capacity by relaxation technique: Calorimeter performance testing and heat capacity of benzo[b]fluoranthene, benzo[k]fluoranthene, and indeno[1,2,3-cd]pyrene. *J. Chem. Thermodyn.* **2020**, *142*, 105964. [[CrossRef](#)]
23. Suzuki, Y.T.; Yamamura, Y.; Sumita, M.; Yasuzuka, S.; Saito, K. Neat liquid consisting of hydrogen-bonded tetramers: Dicyclohexylmethanol. *J. Phys. Chem. B* **2009**, *113*, 10077–10080. [[CrossRef](#)]
24. Archer, D.G. Thermodynamic Properties of the NaCl+H<sub>2</sub>O System I. Thermodynamic Properties of NaCl(cr). *J. Phys. Chem. Ref. Data* **1992**, *21*, 1–21. [[CrossRef](#)]
25. Kresse, G.; Joubert, D. From ultrasoft pseudopotentials to the projector augmented-wave method. *Phys. Rev. B* **1999**, *59*, 1758–1775. [[CrossRef](#)]
26. Perdew, J.P.; Burke, K.; Ernzerhof, M. Generalized Gradient Approximation Made Simple. *Phys. Rev. Lett.* **1996**, *77*, 3865–3868. [[CrossRef](#)] [[PubMed](#)]
27. Knacke, O.; Kubaschewski, O.; Hesselmann, K. *Thermochemical Properties of Inorganic Substances*, 2nd ed.; Springer: Berlin/Heidelberg, Germany, 1991.
28. Tyurin, A.V.; Gavrichev, K.S.; Golushina, L.N.; Gorbunov, V.E.; Zlomanov, V.P. Heat Capacity and Thermodynamic Functions of Ga<sub>2</sub>Se<sub>3</sub> from 14 to 320 K. *Inorg. Mater.* **2005**, *41*, 1139–1143. [[CrossRef](#)]
29. Tyurin, A.V.; Gavrichev, K.S.; Zlomanov, V.P.; Bykova, T.A. Low-temperature heat capacity and thermodynamic functions of Ga<sub>2</sub>Te<sub>3</sub>. *Inorg. Mater.* **2006**, *42*, 954–957. [[CrossRef](#)]
30. Koshchenko, V.I.; Grinberg, Y.K.; Demidenko, A.F.; Zhegalina, V.A. Temperature dependence of thermodynamic properties of indium selenide in the 5–300 K range. *Izv. Akad. Nauk SSSR Neorg. Mater.* **1981**, *17*, 1979–1982.
31. Boehnke, U.C.; Kühn, G.; Berezovski, G.A.; Spassov, T. Some aspects of the thermal behaviour of In<sub>2</sub>Se<sub>3</sub>. *J. Therm. Anal.* **1987**, *32*, 115–120. [[CrossRef](#)]
32. Mills, K.C. Molar heat capacities and enthalpies of transition for the indium selenides, InSe(c), InSe<sub>1.2</sub>(c) and In<sub>2</sub>Se<sub>3</sub>(c). *High Temp. High Press.* **1976**, *8*, 225–230.
33. Zlomanov, V.P.; Sheiman, M.S.; Legendre, B. Phase diagram and thermodynamic properties of phases in the In-Te system. *J. Phase Equilib.* **2001**, *22*, 339. [[CrossRef](#)]
34. Bale, C.W.; Bélisle, E.; Chartrand, P.; Decterov, S.A.; Eriksson, G.; Hack, K.; Jung, I.H.; Kang, Y.B.; Melançon, J.; Pelton, A.D.; et al. FactSage thermochemical software and databases—Recent developments. *Calphad* **2009**, *33*, 295–311. [[CrossRef](#)]
35. Cox, J.D.; Wagman, D.D.; Medvedev, V.A. *CODATA Key Values for Thermodynamics*; Hemisphere Publishing Corp.: New York, NY, USA, 1989.

**Disclaimer/Publisher’s Note:** The statements, opinions and data contained in all publications are solely those of the individual author(s) and contributor(s) and not of MDPI and/or the editor(s). MDPI and/or the editor(s) disclaim responsibility for any injury to people or property resulting from any ideas, methods, instructions or products referred to in the content.